Design of a Novel Pulser for Frequency Selective-based Power and Data Transmission

(Article begins on next page)

03 May 2024

Design of a Novel Pulser for Frequency Selective-based Power and Data Transmission

Stefano Taccetti
ARCES - University of Bologna
40136 Bologna, Italy
stefano.taccetti2@unibo.it

Lorenzo Mistral Peppi
ARCES - University of Bologna
40136 Bologna, Italy
lorenzomistral.pepp2@unibo.it

Federica Zonzini
DEI - University of Bologna
40136 Bologna, Italy
federica.zonzini@unibo.it

Masoud Mohammadgholiha
DEI - University of Bologna
40136 Bologna, Italy
m.mohammadgholiha@unibo.it

Matteo Zauli
ARCES - University of Bologna
40136 Bologna, Italy
matteo.zauli7@unibo.it

Luca De Marchi
DEI - University of Bologna
40136 Bologna, Italy
l.demarchi@unibo.it

Abstract—This paper proposes an ultrasonic system based on an innovative piezoelectric device, the Frequency Steerable Acoustic Transducer (FSAT). The FSAT's high directivity can be exploited for structural inspection, and through-metal data communication and wireless power transfer. These three functions are fundamental in an autonomous sensor system developed for condition monitoring, which is a central requirement in many sectors, such as automotive. A novel pulser, made up of a signal generator and a power amplifier, has been designed and simulated, for effectively driving the FSAT transducer. Experimental results showed that the designed power amplifier is able to reach a gain of $17.80\,\mathrm{dB}$ driving the piezoelectric transducer with a maximum peak-to-peak voltage of $24\,\mathrm{V}$ and that its bandwidth is **[3.1-964] kHz**. Experiments have been carried out showing a great improvement in trasmission using the designed amplifier.

Index Terms—Guided waves pulser, Structural inspection

I. INTRODUCTION

Ultrasonic Guided Waves (GWs) inspections have gained substantial interest in the realm of Structural Health Monitoring (SHM) over the past decades. These inspections involve the usage of multiple piezoelectric transducers to assess the integrity of a component [1], [2]. The need for structural integrity assessment has become crucial in the e-mobility ecosystems with specific emphasis on the automotive sector, since systems are evolving towards more complex geometries and construction materials whose integrity against aging and operational flaws (e.g., cracks, delaminations) requires a special attention. It is worth noting that GW methods has been also proved to be capable of estimating the state of charge of high-energy battery packs [3]. However, the widespread application of such monitoring systems is restricted by weight penalties, complicated circuitry, and maintenance concerns related to extensive wiring. To simplify hardware, reduce costs, and overcome these challenges, Frequency Steerable Acoustic Transducers (FSATs) with inherent directional capabilities can be used instead of traditional piezoelectric transducers [4]. FSATs leverage frequency-dependent spatial filtering effects for beam steering, allowing for 2D surface scanning with minimal software and hardware requirements. Guided waves have also been studied for Ultrasonic Wireless Power Transfer (UWPT) to power up inaccessible sensor nodes and to cut the cost of battery replacement [5]. This solution overcomes problems related to inductive WPT, like the metal shielding effect in standard materials [6]. On the other hand, there are many factors that affect the performances of a UWPT system, which still need to be investigated both through simulations and experiments: the dimensions of the piezoelectric devices, the distance between the power transmitter and the receiver, the transducers coupling with the monitored structure, the electronic circuits for transmitting and receiving power, just to name a few.

A major challenge to be faced in e-mobility oriented monitoring scenario is the capability to ensure, at the same time, low-power and low-cost electronics, reliable data management and information sharing, and trustworthy diagnostics. In particular, WPT has recently emerged as a promising solution to jointly address these three needs: indeed, the energy harvested by the monitoring system during the inspection phase by advanced actuation-transduction solutions can then be used by smart sensor nodes directly attached to the automotive component to i) on-board process and ii) outsource the result of the inspection itself.

A. Related works

An essential part of the inspection system is the design of the pulser, i.e., the electronic circuit used for generating the voltage waveforms that excites the piezoelectric device. This device requires high voltage output, as it is basically used for heightening the power delivered to the final node by increasing the amplitude of the injected signals,

There are four main typologies of ultrasonic pulsers illustrated in literature [7], which can be subdivided in the following categories: drivers and high voltage FETs, integrated chips, multiplexers or switches and, finally, signal generators and power amplifiers. For example, the HDL6V5583 is an ABLIC integrated pulser used in Structural Health Monitoring (SHM)

applications [8]. Conversely, the MD1711 and MD1213 are drivers produced by Microchip and used for Nondestructive Testing (NDT) [9]. However, the two previously mentioned solutions suffer from several drawbacks: on one side, integrated solutions are characterized by large size and costs, while Microchip drivers show high distortion in waveform generation while working in the typical bandwidth of the FSAT (50-450 kHz). As such, a different strategy has been selected in this work, which is based on a signal generator combined with a power amplifier. Indeed, this alternative offers one main benefit, that is the possibility to readily realize the signal generator via the Digital-to-Analog Converter (DAC) of a Microcontroller Unit (MCU), which has the advantages of reduced size and costs but also exhibits great flexibility.

Some preliminary energy transmission tests have already been performed using a pair of FSAT transducers bonded at a $50\,\mathrm{cm}$ distance on a metal plate and driven by a function generator providing a $5\,\mathrm{V}$ peak-to-peak sinusoidal voltage. The results have shown that, under this measurement setup, a maximum value of $79.37\,\mathrm{mV}$ and $49.30\,\mathrm{mV}$ can be measured at the receiving point for an excitation frequency of $50\,\mathrm{kHz}$ and $122\,\mathrm{kHz}$, respectively. Nevertheless, these quantities might be insufficient to ensure power-independent smart sensor functionalities.

Coherently, a novel and dedicated power amplifier is proposed, allowing more power to be transmitted and delivered to the receiving transducer. The pulser is designed to be capable of high-voltage custom waveform generation, to match the voltage and current requirements imposed by the custom piezoelectric load (i.e., the FSAT transducer) that the MCU can't directly generate. In particular, the design of the power stage has been carried out taking care the need of linearity, necessary to minimize the effects of the distortion; a thorough simulation of the amplifier performances has, thus, been performed to prove the functionality of the proposed circuit.

The following section of this paper describes the architecture of the pulser, primarily focusing on the design of the power stage. Then the last part is dedicated to numerical and experimental results.

II. THE POWER STAGE: PULSER ARCHITECTURE

The architecture of the ultrasonic inspection system is based on the piezoelectric actuator, which converts the electrical energy into mechanical energy, and on the waveform generator, which is interfaced with the FSAT through the power stage.

Fig. 1-A illustrates the proposed system architecture on a representative car chassis damage detection application scenario, showing the FSAT transducer and the block diagram of the pulser. In this framework, the UWPT process is used to supply the nodes, as illustrated in Fig. 1-B, their communications and their inspection activity, as illustrated in Fig. 1-C.

A. Signal generator

Concerning the signal generator component, an STM32 MCU has been programmed to generate the voltage waveform for the inspection, comprising rectangular pulses as well as
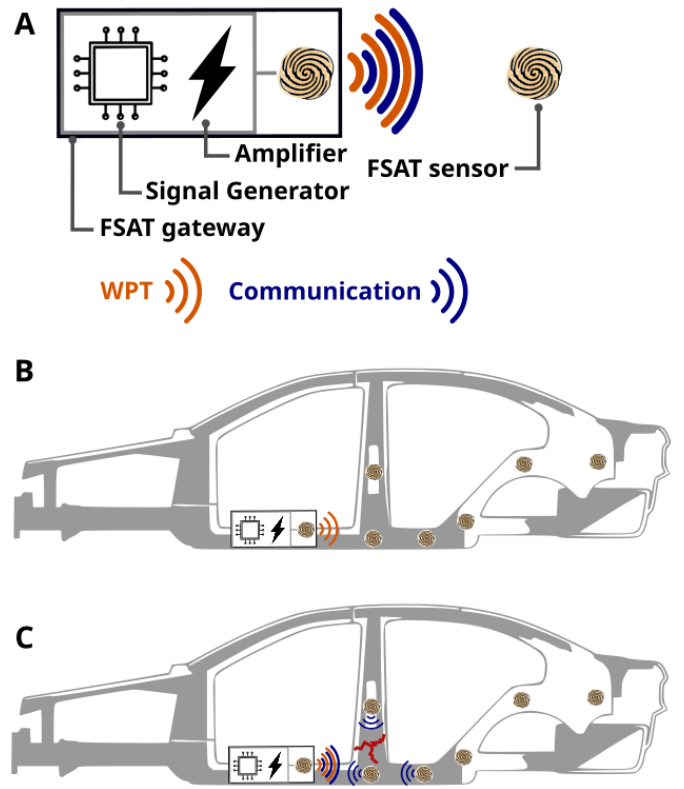

Fig. 1. System architecture and application: A) FSAT gateway (based on Signal generator and Amplifier) and FSAT sensor B) UWPT on car chassis C) UWPT and communication on car chassis for damage inspection

sinusoidal tone bursts modulated by specific windows (e.g., Hann, Hamming), the latter being even more effective [10]. The DAC of the considered STM32 family has a resolution of 12 bits, which means 4096 quantization steps, and it is equipped with an output buffer that can optionally be enabled to minimize the output impedance. Remarkably, this possibility is really beneficial in the design of the power interface.

B. Amplifier design

The power stage design must take care of the maximum value of the output current used for supplying the piezoelectric actuator. Considering the FSAT electrical model, it is equivalent to that of a capacitor of $35\,\mathrm{nF}$: therefore, when applying a sinusoidal voltage to its terminals with a maximum peak-to-peak value of $24\,\mathrm{V}$ and a maximum frequency of $450\,\mathrm{kHz}$, the power stage must supply an output current of at most $1.2\,\mathrm{A}$. Given this requirement, the power operation amplifier OPA564 produced by Texas Instruments has been chosen for the interface, since it is able to drive up to $1.5\,\mathrm{A}$ into a reactive load, operating from dual supply up to $\pm 12\,\mathrm{V}$.

Moreover, in order to maximize the input impedance of the amplifier, a non-inverting configuration is selected, which is illustrated in Figure 2. The gain stage can easily be modified by replacing the feedback resistance value. In this application, four different gain values are considered: 4.72, 5.55, 6.45,
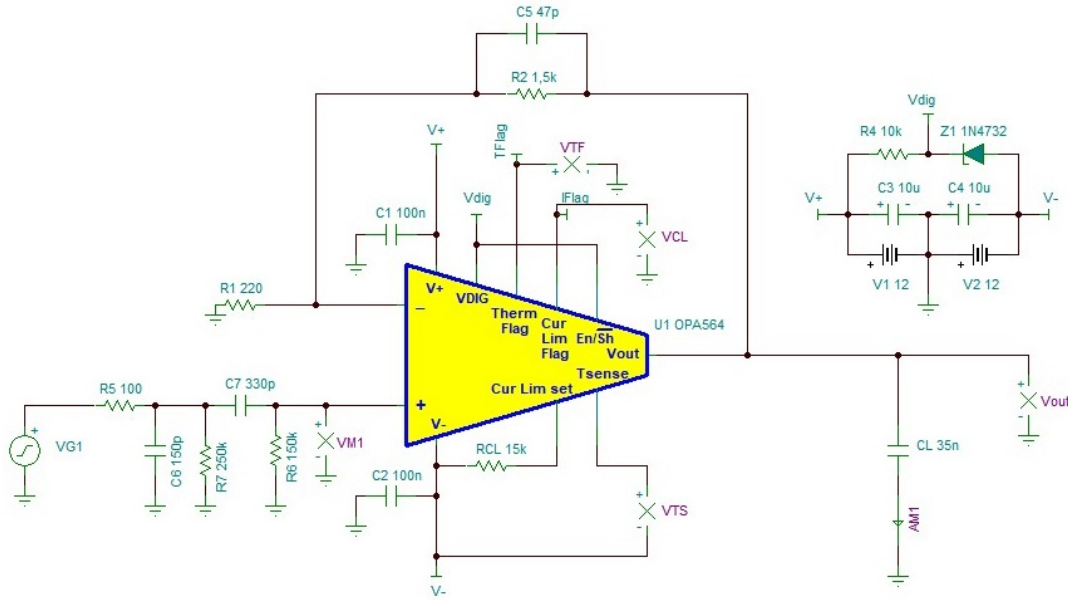
Fig. 2. Amplifier schematic

7.82, which are related to feedback resistances of, respectively, 0.82, 1, 1.2 and $1.5\,\text{k}\Omega$.

The resistance connected to the ISET pin of the OPA564 (Cur Lim set in Fig. 2) is used to set the maximum output current value, e.g., $15\,\text{k}\Omega$ forces a limit of $1.2\,\text{A}$. If the output current exceeds this value, the output flag IFLAG of the OPA564 switches from low to high logic level. The TFLAG shows the same behavior when the die temperature exceeds its limits.

In order to improve stability, a capacitance is added in parallel with the feedback resistor, forming a low pass filter with a cutoff frequency of $2.3\,\text{MHz}$. The bandwidth of this filter is kept constant when the gain changes, so each feedback resistance is connected to a specific parallel capacitance.

A passive band-pass filter was also added as a means to remove the DC component of the DAC-generated waveform and the high frequency components of the input signal [11], without affecting the FSAT working bandwidth. This filter is the cascade of an RC low pass filter, which has a cutoff frequency of $10\,\text{MHz}$, and an RC high-pass filter, having a cutoff frequency of $3\,\text{kHz}$. The DAC output buffer of the microcontroller is enabled so that the DAC output impedance is almost zero and doesn't alter the value of the upper cutoff frequency of the band-pass filter.

III. SIMULATION RESULTS

The TINA-TI software has been used for simulations and verify the functionality of the designed amplification stage.

First, an AC stability analysis has been set to compute the Loop Gain of the amplifier and determine the phase margin. As can be observed in Fig. 3, the system resulted to be stable with a phase margin of $56.2°$ ensured by the feedback capacitor, hence it does not need to be further compensated in frequency.

In fact, adding a simple compensation resistance out of the loop would not improve the phase margin significantly and, conversely, it would add an undesired series inductance which must be cancelled to not alter the frequency response of the stage. As can be seen in Figure 4, the frequency response is flat in the FSAT excitation signal bandwidth.

The system's linearity has been evaluated firstly through Fourier series analysis. To this aim, a sinusoidal signal has been provided as input, hence quantifying the the total harmonic distortion (THD) at the output node by taking into consideration the first N Fourier coefficients. For $N = 15$, the maximum THD resulted equal to 6.4%, scored for a fundamental frequency of $450\,\text{kHz}$.

Then, the transient analysis has been used to check signals variation in time, both in ideal conditions and with an output current exceeding the chosen limit. Fig. 5 illustrates the TINA-TI transient simulation of the amplifier with a nominal gain of 6.45: the green curve corresponds to a $450\,\text{kHz}$ DAC-generated sinusoidal voltage with an amplitude of $1.65\,\text{V}$ and a DC level of $1.65\,\text{V}$, the red curve to the band-pass filtered voltage waveform and the grey curve to the power stage output voltage waveform.

The main features of the designed amplifier are summarized in Table I.

IV. EXPERIMENT AND RESULTS

Since the simulations of the amplifier met the requirements, a printed circuit board has been designed and the device properties have been investigated to compare them with those collected in Table I. The implemented power stage showed a behavior comparable to the one analyzed by TINA-TI, having a maximum gain equal to 7.76 ($17.80\,\text{dB}$) and a frequency

Fig. 3. TINA-TI AC Stability analysis

Fig. 4. TINA-TI AC analysis: output voltage frequency response

Fig. 5. TINA-TI Transient analysis, voltage waveforms: 450 kHz DAC-generated waveform (green curve), band-pass filtered waveform (red curve), amplifier output (grey curve)

TABLE I
AMPLIFIER PROPERTIES

Feature	Description
Supply Voltage (Max)	± 12 V
Output Current (Max)	1.5 A
Input filter Bandwidth	3 kHz - 10 MHz
Nominal Gain	4 Options: 4.72, 5.55, 6.45, 7.82
Phase Margin	56.2°
THD Max (Estimation)	6.4%

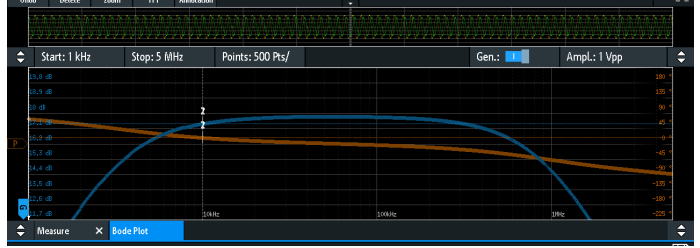response, which is illustrated in Figure 6, very similar to the one simulated (Figure 4.

Fig. 6. Power amplifier measured frequency response

The transmission test has been performed again to inspect the amplifier stage improvement and its capability in driving the FSATs. Figure 7 shows the built experimental setup, emphasizing the FSATs' placement on a metal plate and the way they're driven through the power stage circuit.
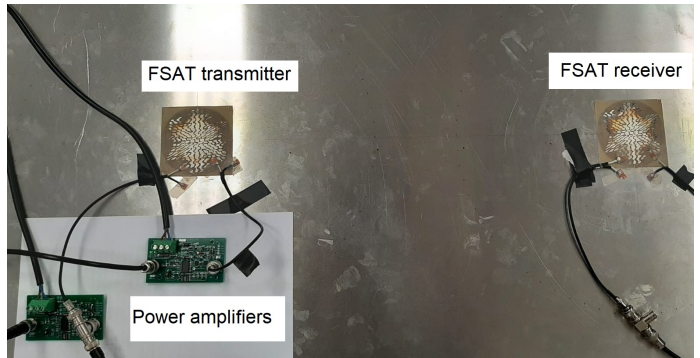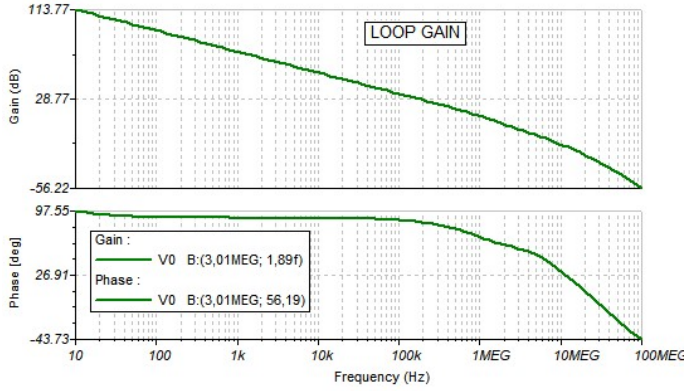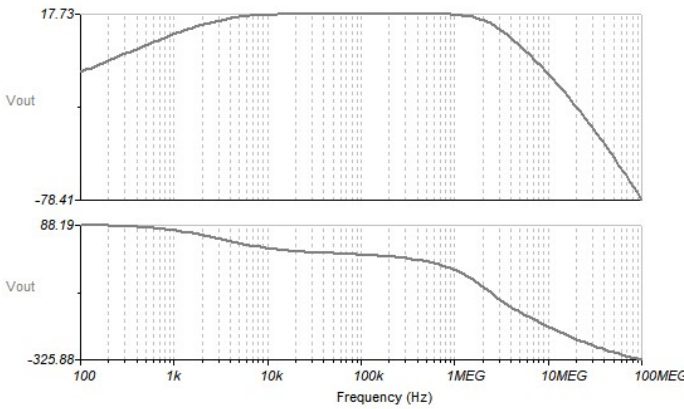

Fig. 7. Experimental set up:1 mm thick aluminum plate with two FSATs at a distance of 50 cm. Each transmission channel is driven by a power amplifier connected to a function generator

A 1 mm thick aluminum plate has been chosen for Lamb waves propagation, placing on its surface a couple of FSATs at a 50 cm distance. Since the generated wave propagation direction depends on the voltage excitation frequency, the transmitter driving signal has to be carefully chosen to maximize the energy received by the second transducer. For this reason, three excitation frequencies have been considered in these experiments: 50 kHz, 83 kHz, 122 kHz, which allow steering the radiation pattern in the direction that links the transmitter to the receiver of Figure 7. A function generator (AFG31000,Tektronix [12]) has been used for generating a

5 cycles sinusoidal burst signal varying the frequency between the three above-mentioned values and the peak-to-peak amplitude from $2\,$V to $5\,$V. The power amplifier has been then introduced between the function generator and the transducer to reach higher peak-to-peak voltage values on the FSATs' electrodes, obtaining a maximum value of $23\,$V as a result of the maximum supply voltage of the OPA564, that is $\pm 12\,$V. Figure 7 points out that every FSAT is accessible by a couple of channels and, when employed for transmission, the two channels' voltages need to be in phase opposition to perform the beam steering action. For this reason, two function generator channels are involved in the experimental setup and two power stages are required for studying the effects of the designed circuit on transmission. The receiver FSAT is also accessible by two channels, generating a couple of voltages that are again in phase opposition. These two received signals are measured by an oscilloscope (RTM3004, Rohde Schwartz [13]), and their difference is then computed, achieving a peak-to-peak differential voltage value that is comparable to the double of each single channel one.

Table II collects results obtained from these experiments, highlighting the dependence of the differential peak-to-peak voltage on the receiver side from the excitation signal frequency and its peak-to-peak amplitude. These results prove the significant improvement in transmission as a result of the introduction of the power amplifier stage,

TABLE II
TRANSMISSION TESTS RESULTS

Frequency [kHz]	Pk-Pk tx voltage [V]	Pk-Pk rx voltage [mV]
50	2	37.86
50	5	79.37
50	23	435.14
83	2	42.60
83	5	151.58
83	23	490.58
122	2	23.15
122	5	49.37
122	23	351.14

V. CONCLUSIONS AND FUTURE WORKS

In this work, a novel power amplifier for DAC-generated signals has been studied and simulated. The proposed pulser is designed to drive a particular piezoelectric device, the FSAT. Thanks to its high directivity, this transducer can be used not only for material inspections, but also for data communication and wireless power transfer, which are of paramount importance for the realization of self-contained, autonomous automotive inspection systems. Simulation results and experimental tests show that the implemented amplification stage can drain up to $1.5\,$A with a voltage swing of $24\,$V and can gain up to $17.80\,$dB, generating an output voltage with an amplitude 7.76 times that of the input voltage. The experiments carried out with the FSATs highlighted the substantial improvement in through-metal transmission brought by the power amplifier. The peak-to-peak differential voltage

measured at the receiver end reached the value of $460.58\,$mV when the FSAT transmitter, at a distance of $50\,$cm, was driven by a $23\,$V peak-to-peak sinusoidal voltage with a frequency of $83\,$kHz.

REFERENCES

[1] Lingyu Yu and Victor Giurgiutiu. In situ 2-d piezoelectric wafer active sensors arrays for guided wave damage detection. *Ultrasonics*, 48(2):117–134, 2008.

[2] Marco Dibiase, Masoud Mohammadgholiha, and Luca De Marchi. Optimal array design and directive sensors for guided waves doa estimation. *Sensors*, 22(3):780, 2022.

[3] Purim Ladpli, Fotis Kopsaftopoulos, and Fu-Kuo Chang. Estimating state of charge and health of lithium-ion batteries with guided waves using built-in piezoelectric sensors/actuators. *Journal of Power Sources*, 384:342–354, 2018.

[4] Masoud Mohammadgholiha, Antonio Palermo, Nicola Testoni, Jochen Moll, and Luca De Marchi. Finite element modeling and experimental characterization of piezoceramic frequency steerable acoustic transducers. *IEEE Sensors Journal*, 22(14):13958–13970, 2022.

[5] Yunfei Xu, Yongshun Sun, Jian Tang, Chao Wei, Xiaoxi Ding, and Wenbin Huang. A lamb waves-based wireless power transmission system for powering iot sensor nodes. *Smart Materials and Structures*, 31(10):105009, aug 2022.

[6] Ding-Xin Yang, Zheng Hu, Hong Zhao, Hai-Feng Hu, Yun-Zhe Sun, and Bao-Jian Hou. Through-metal-wall power delivery and data transmission for enclosed sensors: A review. *Sensors*, 15:31581–31605, 12 2015.

[7] Luc Jonveaux, Jorge Arija, Carla Schloh, Jean Rintoul, and William Meng. Review of current simple ultrasound hardware considerations, designs, and processing opportunities. *Journal of Open Hardware*, 6:1–29, 02 2022.

[8] Pietro Giannelli, Andrea Bulletti, Maurizio Granato, Giovanni Frattini, Giacomo Calabrese, and Lorenzo Capineri. A five-level, 1-mhz, class-d ultrasonic driver for guided-wave transducer arrays. *IEEE Transactions on Ultrasonics, Ferroelectrics, and Frequency Control*, 66(10):1616–1624, 2019.

[9] Jian-Xing Wu, Yi-Chun Du, Chia-Hung Lin, Pei-Jarn Chen, and Tain-song Chen. A novel bipolar pulse generator for high-frequency ultrasound system. In *2013 IEEE International Ultrasonics Symposium (IUS)*, pages 1571–1574, 2013.

[10] Jianlin Chen, Zheng Li, and Kezhuang Gong. Nondestructive testing method based on lamb waves for localization and extent of damage. *Acta Mechanica Solida Sinica*, 30(1):65–74, 2017.

[11] Douglas Self. Chapter 14 - line inputs. In Douglas Self, editor, *Small Signal Audio Design*, pages 339–380. Focal Press, Boston, 2010.

[12] *Tektronix Arbitrary Function Generators AFG31000.* https://download.tek.com/datasheet/AFG31000-Arbitrary-Function-Generators-Datasheet-75W614443.pdf.

[13] *RS RTM3000 OSCILLOSCOPE.* https://scdn.rohde-schwarz.com/ur/pws/dl_downloads/dl_common_library/dl_brochures_and_datasheets/pdf_1/RTM3000_dat_en_5214-9144-32_v0700.pdf.